Corrigendum

Linkage mechanics and power amplification of the mantis shrimp's strike

S. N. Patek, B. N. Nowroozi, J. E. Baio, R. L. Caldwell and A. P. Summers

10.1242/jeb.052274

There was an error published in *J. Exp. Biol.* **210**, 3677-3688.

In Eqn 1 on p. 3680, a '+' sign was used instead of the correct '–' sign. The equation is shown in its corrected form below.

$$L_{db} = \sqrt{L_2^2 + L_1^2 - 2L_1L_2\cos(\theta_{input})}\ , \qquad (1)$$

The authors apologise for this error but assure readers that the correct equation was used in the calculations that form the results reported in the study.

The Journal of Experimental Biology 210, 3677-3688
Published by The Company of Biologists 2007
doi:10.1242/jeb.006486

Linkage mechanics and power amplification of the mantis shrimp's strike

S. N. Patek[1,*], B. N. Nowroozi[2], J. E. Baio[1], R. L. Caldwell[1] and A. P. Summers[2]

[1]*Department of Integrative Biology, University of California, Berkeley, CA 94720-3140, USA and* [2]*Ecology and Evolutionary Biology, University of California–Irvine, Irvine, CA 92697-2525, USA*

*Author for correspondence (e-mail: patek@berkeley.edu)

Accepted 6 August 2007

Summary

Mantis shrimp (Stomatopoda) generate extremely rapid and forceful predatory strikes through a suite of structural modifications of their raptorial appendages. Here we examine the key morphological and kinematic components of the raptorial strike that amplify the power output of the underlying muscle contractions. Morphological analyses of joint mechanics are integrated with CT scans of mineralization patterns and kinematic analyses toward the goal of understanding the mechanical basis of linkage dynamics and strike performance. We test whether a four-bar linkage mechanism amplifies rotation in this system and find that the rotational amplification is approximately two times the input rotation, thereby amplifying the velocity and acceleration of the strike. The four-bar model is generally supported, although the observed kinematic transmission is lower than predicted by the four-bar model. The results of the morphological, kinematic and mechanical analyses suggest a multi-faceted mechanical system that integrates latches, linkages and lever arms and is powered by multiple sites of cuticular energy storage. Through reorganization of joint architecture and asymmetric distribution of mineralized cuticle, the mantis shrimp's raptorial appendage offers a remarkable example of how structural and mechanical modifications can yield power amplification sufficient to produce speeds and forces at the outer known limits of biological systems.

Key words: power amplification, predation, movement, feeding, speed, acceleration, Crustacea, kinematic transmission, four-bar linkage model.

Introduction

All animals face an overriding constraint on their ability to produce fast movements – muscles contract slowly and over small distances. Repeatedly over evolutionary history, animals have overcome this limitation through the use of power amplification mechanisms. These mechanisms decrease the duration of movement and thereby increase speed and acceleration (Alexander, 1983; Alexander and Bennet-Clark, 1977; Gronenberg, 1996a). Power-amplified animal movements are truly diverse, ranging from the elastic tendons and springy legs of kangaroo and locust jumps, to snapping shrimp appendages and spring-loaded vertebrate ballistic tongues (Alexander, 1990; Alexander and Bennet-Clark, 1977; de Groot and van Leeuwen, 2004; Deban et al., 1997; Heitler, 1974; Lappin et al., 2006; Nishikawa, 1999; Ritzmann, 1973; Versluis et al., 2000).

In all of these systems, relatively slow muscle contractions precede rapid movement. As muscles contract to provide the necessary work for the movement, elastic potential energy is typically stored in structural elements (e.g. kangaroo tendons) while latches and/or antagonistic muscle contractions prevent movement until the animal is ready to jump or strike (Alexander, 1983; Gronenberg, 1996a). A good analogy for these biological principles is found in the crossbow: slow muscle contractions of a human arm gradually load ('load phase') and store elastic potential energy in the crossbow and ultimately a latch releases the string, which in turn drives forward the arrow ('release phase'). In the load phase, muscle contractions load elastic elements and thereby store potential energy. In the release phase, fast movement is actuated through the rapid release of stored potential energy. It is important to note that in the release phase, muscle activity plays a minimal role or no role at all in actuating the fast movement; the release of elastic potential energy occurs at far shorter timescales than muscle contractions. With this mechanism, the arrow accelerates and flies through the air at far greater speeds than would have been possible by simply throwing the arrow.

The mysteries of the crossbow – where is energy stored, how release is triggered, and the mechanics behind the loading or unloading of the bow – are the same principal questions we ask of a biological energy storage system. The speed and power of the killing strike of the second thoracic appendages (the 'raptorial appendages') of mantis shrimp (Stomatopoda) are clear evidence of a power amplification system at work (Fig. 1) (Burrows, 1969; Patek and Caldwell, 2005; Patek et al., 2004). The entire strike occurs over several milliseconds and can reach peak speeds of 10–24 m s^{-1} (Burrows, 1969; Burrows and Hoyle, 1972; Patek et al., 2004). Peacock mantis shrimp *Odontodactylus scyllarus* can directly deliver impact forces of over 1000 N (thousands of times its body weight) with an equal or greater force secondarily caused by cavitation bubble collapse (Patek and Caldwell, 2005).

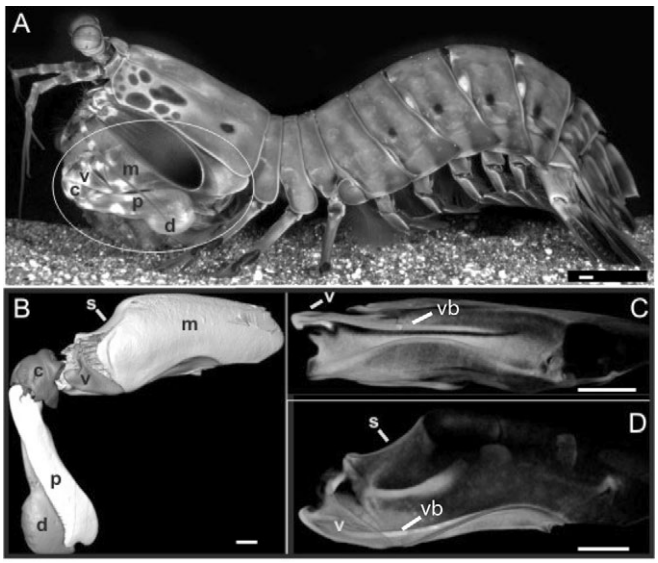

Fig. 1. *Odontodactylus scyllarus* raptorial appendage. (A) A resting peacock mantis shrimp with the raptorial appendage circled. Raptorial appendages are used either for stabbing (dactyl open and extended) or for hammering (dactyl folded in and bulbous heel exposed, as shown here). (B) Lateral view of an isosurface rendering of segmented CT scan data of the left raptorial appendage. Each skeletal element has been pseudocolored to increase contrast. The isosurface threshold has been optimized for each element to illustrate the morphology and spatial relationships. (C) Ventral view of a shadowless volume rendering of left merus (m). Shading corresponds to degree of radio-opacity (mineralization), with lighter colors corresponding to greater mineralization and darker to poorly mineralized areas. Note the unmineralized region adjacent to the highly mineralized ventral bar (vb) extending proximally from the base of the meral-V. This unmineralized region may permit dorso-proximal flexion of the meral-V (v). (D) Lateral view of the merus using the same rendering technique as in C. s, saddle; c, carpus; p, propodus; d, dactyl. Scale bars, 4 mm.

Mantis shrimp, like all crustaceans, control movement with antagonistic pairs of muscles that alternately abduct and adduct their appendages. However, in the load phase of a power-amplified strike, mantis shrimp simultaneously activate the antagonistic muscles connecting the carpus and merus segments in the raptorial appendage as they prepare for a high-powered strike (Fig. 1). Specifically, they contract large, slow extensor muscles in the merus while contracted flexor muscles in the merus brace a pair of sclerites to prevent movement (Burrows, 1969; Burrows and Hoyle, 1972; McNeill et al., 1972). When the extensor muscles have fully contracted and the animal is ready to strike, the flexor muscles turn off, releasing the sclerites, and the appendage rapidly rotates outward toward its target (Burrows, 1969; Burrows and Hoyle, 1972; McNeill et al., 1972). It has been proposed that energy is stored in a saddle-shaped portion of the merus exoskeleton (Patek et al., 2004) and in the connective tissue of merus, specifically the extensor muscles and apodemes (Burrows, 1969).

The morphological complexity and evolutionary diversity of the mechanical system that drives the raptorial strike raises the possibility that there is a leverage system, such as a four-bar linkage, underlying the rapid rotation of the dactyl. While the storage and release of cuticular elastic energy during the release phase is often observed in arthropods, e.g. locust jumping legs (Heitler, 1974), linkage mechanisms in arthropod power amplification mechanisms are not well studied. These jointed leverage systems amplify rotational motion and are typically characterized in terms of kinematic transmission (KT; angular output of the linkage mechanism divided by angular input) (Barel et al., 1977; Westneat, 1994) (Fig. 2). Thus, KT provides a heuristic measure of speed- *versus* force-modification of the linkage system, such that a high KT system delivers a large angular output (e.g. angular velocity) for a small angular input and can therefore be considered 'angular velocity-modified' (in the same sense that the mechanical advantage provided by a long output lever relative to input lever is speed-modified). Linkage models of fish jaws have proved to be powerful tools for examining the evolution and performance in force- *versus* speed-modified feeding mechanisms within and across species (Alfaro et al., 2004; Collar et al., 2005; Hulsey and Wainwright, 2002; Muller, 1996; Westneat, 1991; Westneat, 1995; Westneat et al., 1993).

Previous studies have examined the functional morphology of the stomatopod's raptorial appendage (Burrows, 1969; Kunze, 1981), muscle anatomy and activity patterns during the strike (Burrows, 1969; Burrows and Hoyle, 1972; McNeill et al., 1972), and a proposed linkage system and energy storage mechanism (Patek et al., 2004). Here, we build on these previous studies by examining the raptorial morphology and mechanics of peacock mantis shrimp *Odontodactylus scyllarus* from several new perspectives, including the use of CT scan technology to characterize cuticular mineralization patterns and functional morphology of the latches as well as high-speed video analysis to measure changing conformations of the appendage segments and strike kinematics. In addition, we quantitatively test the previously proposed linkage mechanism (Patek et al., 2004) and assess whether the proposed elastic energy storage mechanism could function given the mineralization patterns of the merus.

The goals of the present study were to examine the anatomy of the raptorial appendage and the kinematics of the release phase of the strike mechanism from these functional perspectives. (1) Energy storage: what is the distribution of mineralization in the merus and how does this mineralization pattern contribute to the elasticity and stabilization of the appendage? (2) Latching mechanism and pre-strike stabilization: what are the shapes and orientations of the sclerites and how might they control the preparation for and release of the strike? (3) Kinematic transmission: does a four-bar exoskeletal linkage system mediate the storage and release of potential energy in this system?

Materials and methods

Odontodactylus scyllarus L. (Crustacea, Stomatopoda, Gonodactyloidea, Odontodactylidae) specimens (11.5–14.8 cm body length) were purchased from aquarist companies and housed in re-circulating saltwater tanks (25–30°C). They were fed a diet of fresh snails, frozen shrimp and vitamin-fortified freeze-dried shrimp.

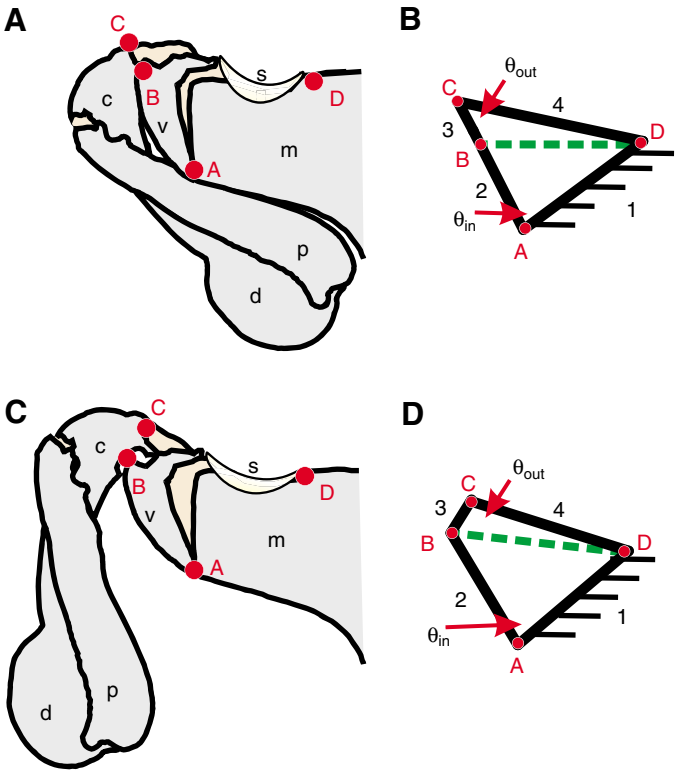

Fig. 2. A four-bar linkage model and the associated points in the proposed mantis shrimp four-bar linkage model. Red circles indicate pivot points; numbers indicate links. Pivots A and D are fixed in space and form Link 1. Link 2 is the input link formed by pivots A and B. Link 3 is the coupler link formed by pivots B and C. Link 4 is the follower link formed by pivots C and D. The input angle (θ_{in}) and output angle (θ_{out}) can be calculated using the law of cosines and the length of the diagonal (green broken line connecting pivots B and D). This particular model configuration is not operational when B, C and D are collinear, thereby limiting the input range of θ_{in} (see Fig. 9 in the Results). (A) A tracing of a high-speed video image of a raptorial appendage that has completed the load phase and is spring-loaded and prepared to strike. The saddle (s) is compressed and the meral-V (v) is rotated proximally. (B) The corresponding linkage model to A. (C) A raptorial appendage in the release phase. The saddle is hyper-extended into a flattened shape. The meral-V is fully rotated and open. (D) The corresponding linkage configuration to C. m, merus; c, carpus; p, propodus; d, dactyl. Beige regions in A and C represent arthrodial membrane; gray regions indicate exoskeleton; yellow area represents the saddle.

Merus mineralization and sclerite functional morphology

Through dissections, computed tomography (CT) scans, manipulations and digital image analysis, we examined the functional morphology of the sclerites and mineralization patterns of the merus, and characterized the articulations connecting the merus and carpus, using a DFC350 FX digital camera and MZ 12.5 microscope (Leica Corp., Germany) and custom digital imaging software (Matlab, The Mathworks, Natick, MA, USA).

Mineralization patterns were visualized using 3-D reconstructions of CT scans (Amira software, v. 3.1.1, Mercury Computer Systems, Berlin, Germany). A freshly frozen individual was micro-CT scanned at the University of Texas with a slice thickness of 0.0585 mm. Slice images were reconstructed at a resolution of 1024×1024 pixels over a 50 mm field of view. Voxels were 0.0488×0.0488×0.0585 and bit depth was either 8 or 16, depending on the need for visualizing soft tissue. The elements of the raptorial appendage were segmented out of the CT scans and separate images of each were created. Isosurface renderings were utilized to show the outer surfaces of each structure and the articulations between these structures. These surface renderings were also useful in identifying areas of reduced mineralization. In addition, volume renderings of each structure were created to further visualize areas of greater and lesser mineralization. In volume rendered images, brighter structures are more highly mineralized. From the surface renderings a VRML file was used as input to a rapid prototype 3-dimensional printer (Z-Corp 310, Burlington, MA, USA) to produce large-scale models of each structure. These models were helpful in deciphering the articulations between the different structures of the raptorial appendage.

Transmission: kinematics and linkage mechanics

We analyzed high-speed images of raptorial strikes and noted the changing configurations of the merus in order to characterize the dynamics of the flexible elements and linkages of the raptorial appendage. Animals regularly struck objects coated with shrimp paste and most animals were willing to strike objects under bright video lights after a period of training. A high-speed imaging system (5000 frames s^{-1}, 35 μs shutter speed; 640×480 pixel resolution; HG100K Redlake Systems, San Diego, CA, USA) recorded stomatopods striking a snail shell coated in shrimp paste and wired to a stick. The snail shell was presented to animals within confined burrows and aligned parallel to the glass wall of the aquarium, thereby allowing us to film strikes with the animal positioned laterally. Sequences in which strikes were directed out of the camera's plane of view were excluded from the dataset.

The following parameters were measured using high-speed imaging: angular velocity, acceleration and strike duration of the dactyl heel (the bulbous structure at the base of the dactyl segment of the raptorial appendage; Fig. 1) (50–58 strikes; 6 individuals; 7–12 strikes per individual), and rotation of the meral-V (a moveable element in the merus segment of the raptorial appendage; Fig. 1) (24 strikes; 6 individuals; 3–7 strikes per individual) (Matlab v. 6.5 and v. 7.0.4). Meral-V rotation was calculated by measuring the change in angle of the meral-V relative to horizontal across each video frame. The acceleration and speed of the dactyl heel were derived from the arc distance traveled by the heel across video image intervals. Two points were digitized along the propodus/dactyl axis formed by the distal two segments of the raptorial appendage, which remain folded during a smashing strike (Fig. 1). The angular change of this line was calculated across video frames. This angle was multiplied by the distance between the propodus/carpus joint and dactyl/propodus joint, which yielded the arc distance moved by the heel of the dactyl.

Speed and acceleration were calculated as the first and second derivatives of distance, respectively. A drawback to computing derivatives from kinematic data is that they only provide average kinematic estimates. Even with curve-fitting and spline methods

(e.g. Walker, 1998), the transient and non-sinusoidal movement of the mantis shrimp's strike caused the filtered and smoothed data to fail to track the displacement of the appendage. Specifically, the movement of the limb follows a gradual path interrupted by a sudden impact and reverse in direction. The smoothing and spline algorithms applied to these data failed to track this transient movement and instead continued to follow the initial path of the appendage. Nonetheless, the animals typically struck the target when the appendage was moving the greatest distance in the arc and the frame rate of 5000 frames s^{-1} under-sampled the movement. Thus, the distances measured were underestimates and the resulting velocities and accelerations should also underestimate the rate of movement. Given the uncertainty of deriving accelerations from these data, we report acceleration in orders of magnitude. The relative movement across frames was converted to SI units by measuring the pixel distance of known structures on the raptorial appendage in each frame and converting pixels to meters using the calibrated distance. We estimated digitizing measurement error by digitizing 5 sequences, 10 times each.

Four-bar linkage pivot points were identified based on high-speed videos, functional morphological observations and manual manipulations of the specimens. Using a standard four-bar linkage configuration (Uicker et al., 2003; Westneat, 1990), we identified four pivot points defining four 'links': a fixed link, input link, follower link and coupler link (Fig. 2, also see Results). We measured link lengths using photographs of raptorial appendages at rest (13 individuals) and in digital video images when all the pivot points were visible (images from 21 video sequences of strikes performed by 4 individuals). Using *t*-tests (JMP v. 5.0.1), we tested whether specimen measurements were equivalent to video-based measurements. In addition, we compared the length of Link 4 between these two datasets, given that Link 4 is formed by the contracted extensor muscle and, therefore, should be longer in the photographs of relaxed appendages than in the video images of appendages prepared to strike.

Based on the above morphological and kinematic analyses, we tested the hypothesis that a four-bar linkage system mechanically couples this system (Fig. 2). With the known length of the diagonal bar (Fig. 2), the law of cosines was used to calculate the angles between any of the links during a given input bar rotation. The lengths of each of the four links (L_n) and the input angle of between $link_1$ and $link_2$ (θ_{input}) were entered into the following equations to calculate the length of the diagonal bar (L_{db}) (Fig. 2):

$$L_{db} = \sqrt{L_2^2 + L_1^2 + 2L_1L_2\cos(\theta_{input})}\,, \quad (1)$$

which was then used to calculate the output angle between $link_3$ and $link_4$ (θ_{output}):

$$\theta_{output} = \arccos[(L_3^2+L_4^2-L_{db}^2)\,(2L_3L_4)^{-1}]\,. \quad (2)$$

Depending on the relative lengths of the links, a four-bar linkage system may allow a 360° rotation of the input link, but a more common case is that the input link 'jams' after some amount of rotation. This range of input angles for which there is movement of the output link is called the 'operational' range of the four-bar linkage. We used a mathematical model to determine the operational range of the input linkage and compared it to the input range actually used by the mantis shrimp. The input range used by the mantis shrimp yielded an output of the four-bar model that was effectively approximated as a line (see Results) with a slope equivalent to the predicted KT of the system.

We statistically evaluated the fit between the predicted four-bar model behavior and the measured kinematics of the raptorial appendage. Given that the carpus, propodus and dactyl are tightly coupled once the dactyl begins to sweep toward its target, we assumed that these three segments share the same pivot point and rotate an equivalent number of degrees during the sweeping phase of the strike. This allowed us to measure the rotation of the propodus as the output angle equivalent to the rotation of Link 3 (carpus); the propodus is larger, visible in a greater proportion of video sequences and can be more accurately digitized than the carpus. We tested whether the slope of the relationship between the input (Link 2) and output angles (Link 3=propodus rotation) measured from the high-speed videos was significantly different than the slope predicted by the four-bar model [modified *t*-test, see p. 32, Grafen and Hails (Grafen and Hails, 2002)]; incorporating individual effects and treating video sequences nested within individuals as random effects using Residual Maximum Likelihood method in JMP statistical software (v. 5.0.1).

Results

Sclerite functional morphology

Stomatopods have two sclerites, sclerite 1 and sclerite 2, which serve as 'latches' to adduct and hold the carpus, propodus and dactyl against the merus while the extensor muscles contract in preparation for a strike (Figs 3, 4) (Burrows, 1969). In *O. scyllarus*, sclerite 1 is a small, rod-shaped structure positioned medially along the ventral edge of the merus and embedded in the thick arthrodial membrane that connects the merus and carpus (Figs 3, 4). The medial flexor apodeme attaches just below the sclerite's tip and forms a thin, pinnate layer over the medial surface of the merus.

Just lateral to sclerite 1, sclerite 2 has a surface that articulates with an infolding of the merus and sweeps through an arc both into and out of the merus (Figs 3, 4). The lateral flexor muscle attaches to the proximal edge of the sclerite and extends *via* a large pinnate muscle to attach to the ventral floor of the merus. When this muscle is manually pulled in a proximal direction, sclerite 2's articulating surface slides smoothly over the infolding of the merus such that it is braced in place, but not latched. When released, the sclerite again slides smoothly along the articulating meral surface and permits abduction of the carpus. When not engaged, sclerite 2 protrudes through the ventral meral-carpal arthrodial membrane and is visible from the outside of the animal (Fig. 4). Both the meral infolding, which forms the brace, and the long axis of the sclerite, are oriented slightly medially. Thus, when sclerite 2 is released, it swings dorsally and medially.

Merus mineralization and articulations

The joint articulations between the merus and carpus range from robust to nearly absent (Figs 3, 5). The lateral meral-carpal articulation is visible externally and is only loosely articulated

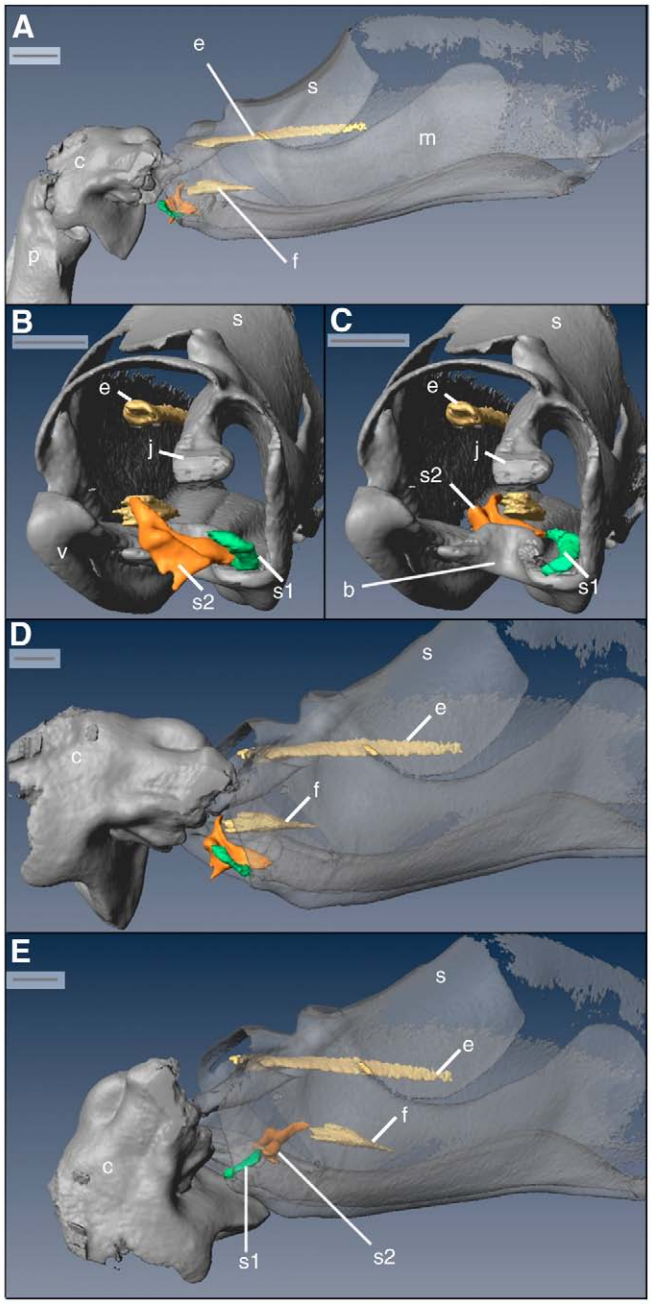

Fig. 3. CT scans of the internal anatomy of the raptorial appendage and the degree of mineralization of the merus exoskeleton (gray is mineralized; transparent regions represent relatively unmineralized exoskeleton). (A) Medial view of the raptorial appendage (proximal to right of page; ventral toward the bottom of the page) showing the large lateral extensor apodeme (e). Ventrally, the lateral flexor apodeme (f) attaches to sclerite 2 (orange). Medial to sclerite 2 is the small, rod-shaped sclerite 1 (green). (B) An internal perspective of the merus viewed from the distal end (lateral to left). Sclerite 2 (s2) is in its resting, unlocked position such that it hangs externally between the merus and carpus. The surface of the distal meral-V (v) articulation, which loosely articulates with the carpus, contrasts with the large internal joint, which forms the medial carpus joint articulation (j). (C) Same view as in B with sclerite 2 and sclerite 1 (s1) in closed and braced positions. Note that sclerite 1 does not appear to directly articulate with sclerite 2 when in the closed position and instead folds medially relative to the edge of sclerite 2. (D) Sclerites in resting position (medial view; distal to left). (E) Locked positions of the sclerites with the carpus rotated counter-clockwise in preparation to strike (medial view). m, merus; c, carpus; s, saddle; p, propodus; b, ventral infolding of merus. Scale bars, 4 mm.

(Fig. 5A). Opposing this somewhat unconstrained connection on the lateral side are two medial meral-carpal articulations (Fig. 5B,C). The internal medial articulation forms a smooth, channel-like surface with a stop at the end, which both stabilizes the carpus to move only along the dorso-ventral axis and also prevents the carpus from adducting beyond a particular angle.

The lateral and medial sides of the merus are distinctly asymmetric in terms of mineralization and flexibility. The medial side is stiff and robust whereas the lateral side is thin and flexible (Figs 1, 3, 5). Similarly, the dorsal surface is thin and flexible while the ventral surface consists of large, stiff buttresses running along the distal-proximal axis. There are also unmineralized regions on the medial and dorsal surfaces where cuticle is replaced by arthrodial membrane.

There are two independently mobile components of the merus' cuticle – the meral-V and the saddle (Figs 5, 6). The meral-V is a thick, triangular-shaped structure that connects to one of the large ventral buttresses forming the underside of the merus. It has a flexion point along the ventral-lateral margin of the merus, such that the meral-V bends at this junction and rotates proximally (Figs 1, 5, 6). The meral-V is flanked by arthrodial membrane and the ventral buttress also has a region of low-mineralization adjacent to it (Fig. 1), allowing this structure room to flex.

Located on the dorsal surface of the merus, the saddle is constructed of poorly mineralized cuticle with thin, flexible arthrodial membrane on its medial and lateral sides (Figs 1, 5, 6). During the load phase, the saddle is compressed and forms a more concave curve along the proximo-distal axis (Fig. 6). At the same time, the saddle rotates slightly ventrally around its proximal connection to the merus and articulates with a notch on the medial side of the merus (Fig. 5B). In the release phase, the saddle rotates dorsally and hyper-extends into a more flattened shape before returning to its initial form (Figs 6, 7).

The saddle and meral-V are connected by a thickened strip of exoskeleton, the meral bridge (Figs 5, 6). When the meral-V is rotated proximally during contraction of the extensor muscles, the meral bridge is pushed proximally and the saddle is simultaneously compressed and rotated (Fig. 6). There are no muscle attachments to the saddle itself. When the saddle, bridge and merus are released from their compressed positions, the tip of the meral-V pushes through its sliding articulation with the lateral side of the carpus, such that the carpus, propodus, and dactyl rotate outward toward the target (Figs 6, 7).

Transmission: kinematics

At the onset of a strike, the propodus and dactyl slide distally along the merus and then transition to a sweeping movement with a large rotational velocity (Figs 7, 8). The duration of the sweeping movement averaged 1.8±0.4 ms (± s.d.) and the sliding movement averaged 0.9±0.5 ms (6 individuals, 6–12 strikes per individual). The dactyl heel reached peak speeds of

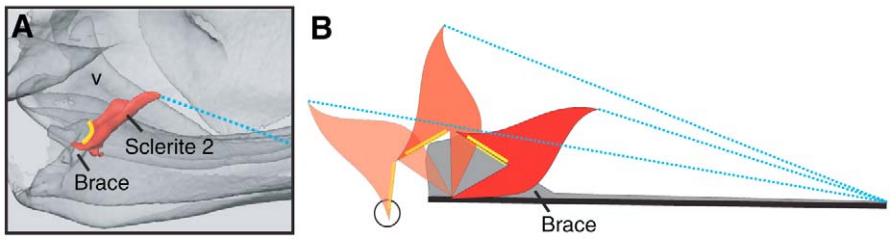

Fig. 4. Sclerite engagement and orientation. (A) Sclerite 2 (red, solid fill) is in the engaged position and braced against the ventral meral infolding. Yellow highlighting indicates the area of ventral meral infolding against which the sclerite is braced. The blue dotted line shows the approximate attachment point and orientation of the lateral flexor muscle that engages the sclerite. Shown from the medial side, with the meral-V (v) behind the sclerite. Ventral is toward the bottom of the page and proximal is to the right. (B) A schematic diagram of the engaged and resting positions of sclerite 2. The darkest sclerite (red) is shown in the engaged position with yellow highlighting the articulating surfaces. When the sclerite is released it rotates distally (to left), to rest with the articulating surface hanging outside the animal (circled). This portion of the sclerite is visible in mantis shrimp specimens and hangs between the merus and carpus. Blue dotted lines show the approximate orientation and attachment of the lateral flexor muscle.

14.7–23.5 m s^{-1} (mean peak speed: 13.7±3.3 m s^{-1}; mean median speed: 3.4±1.7 m s^{-1}), peak angular speeds of 670–990 rad s^{-1} (mean peak angular speed: 608.9±147.0 rad s^{-1}; mean median angular speed: 155.7±79.6 rad s^{-1}), and mean peak accelerations on the order of 10^4 m s^{-2}. Digitizing measurement error at maximal speeds was on average ±4%.

The rotation of the dactyl heel and meral-V were variable and correlated with each other. In all sequences, the dactyl heel struck the prey item while the meral-V was still rotating; thus, during these smashing strikes, the propodus and dactyl did not transition to a ballistic, unpowered phase prior to impact. The dactyl heel struck the snail across a range of excursion angles, such that in some strikes the dactyl/propodus rotated outward only 7° whereas in other strikes the dactyl struck the snail with a maximum extension of 42° (mean: 25±9°). Similarly, the net meral-V rotation ranged widely depending on the excursion of the dactyl when it struck the snail. The net meral-V rotation was on average 9° (range: 3–17°; ±5° s.d.; 5 individuals, 4–6 strikes per individual) (Fig. 7). Values were not significantly different across individuals for propodus rotation (one-way ANOVA; F=0.6943; P=0.60) nor for meral-V rotation (one-way ANOVA; F=1.1424; P=0.37).

Transmission: linkage mechanics

The structural asymmetries of the merus, as described above, generate two distinct functional regions of the merus. Specifically, the robust mineralization and paired meral-carpal articulations on the medial side yield stability and resistance to flexion. By contrast, on the lateral side of the merus, considerable flexion occurs *via* the rotating meral-V, which allows transmission of forces distally to the carpus and proximally to the meral bridge and saddle. It is on this lateral side of the merus that we identified the four-bar linkage system which actuates the spring-loaded raptorial strike during the release phase (Figs 2, 8).

The links comprising the four-bar linkage model are designated as follows (Fig. 2): Link 1, fixed link: proximal merus exoskeleton; Link 2, input link: meral-V; Link 3, coupler link: carpus; and Link 4, follower link: contracted extensor muscle. Previous work showed that the lateral extensor muscle

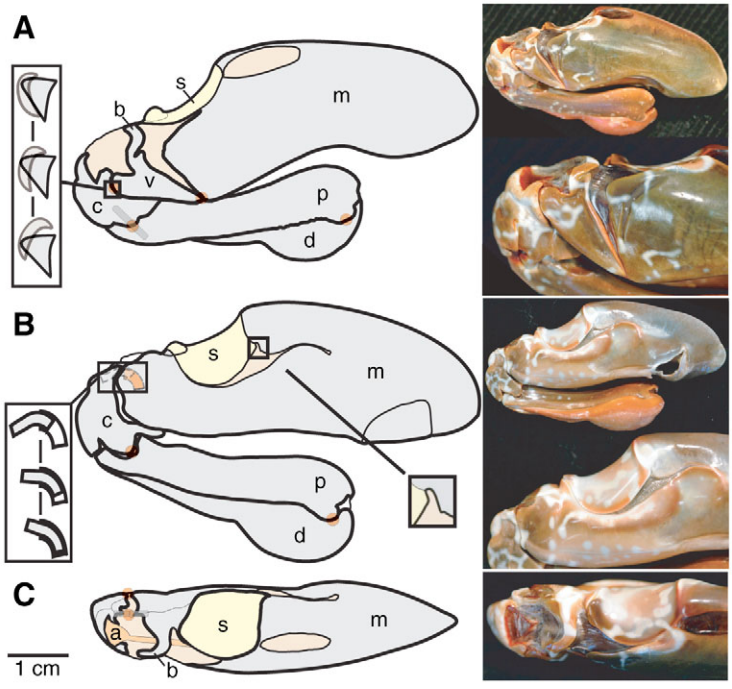

Fig. 5. The morphology of the raptorial appendage of the peacock mantis shrimp. Line drawings are presented adjacent to photographs of the corresponding areas of the raptorial appendage. Proximal is to the right of the page. (A) Lateral view highlights the external, loose articulation between the meral-V (v) and carpus (c; inset). A thin strip of exoskeleton forms the bridge (b) between the meral-V and saddle (s). (B) Medial view shows the internal meral-carpal articulation that functions as a sliding channel joint (left inset). Also visible is the proximal saddle notch, into which the saddle is pushed during extensor muscle contraction in the load phase (right inset). (C) Dorsal view (medial toward top of page) shows the orientation of the lateral extensor apodeme (a, pink) extending from the carpus and running beneath the saddle. The bridge (b) runs dorsally from the lateral meral-V (visible in A) and across to the distal horn of the saddle (visible in B). The medial meral-carpal articulation consists of two adjacent articulations (orange circles); the internal medial meral-carpal articulation is a robust sliding channel joint (as shown in B, left inset). (A–C) Orange circles indicate articulations; gray bars indicate internal buttressing; beige regions are arthrodial membrane; gray regions indicate exoskeleton; yellow coloration represents the saddle (s). m, merus; p, propodus; d, dactyl.

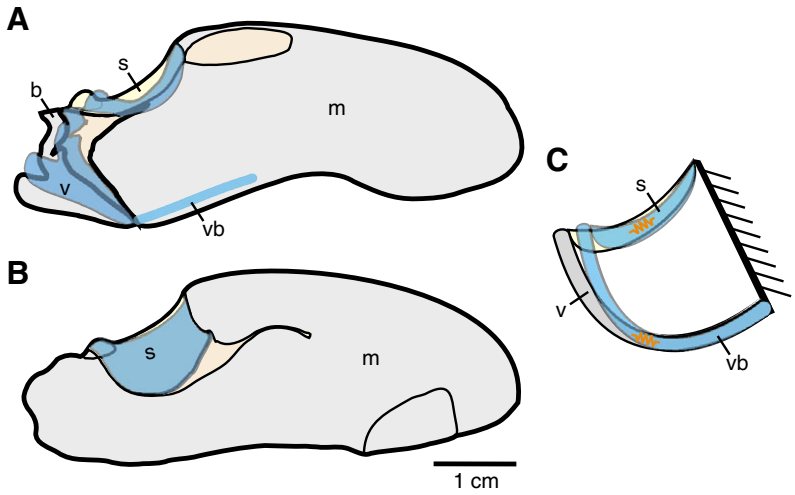

Fig. 6. A resting (solid outline) and loaded (light-blue overlay) merus segment (m) of the raptorial appendage. Proximal is to the right of the page, dorsal is toward the top of the page. (A) Lateral view of the raptorial appendage. When the extensor muscles contract in preparation for a strike in the load phase, the meral-V (v) rotates proximo-medially (clockwise in this image), which simultaneously causes the bridge (b) to move proximally. When the bridge pushes proximally, it pushes against the saddle (s), which is compressed to form a more concave curve. A mineralized ventral bar (vb) extends proximally from the base of the meral-V. (B) Medial view of the raptorial appendage showing the proximal movement and flexion of the saddle caused by extensor muscle contraction. When seen from the medial view, the saddle is pushed into a notch on the merus. (C) A diagram of the possible areas of elastic energy storage (orange spring icons) during rotation of the merus and flexion of the saddle in preparation for a strike. Here we propose that the meral-V functions as a spring by flexing along its base, similar to a tape spring, to form a tighter curve during extensor muscle contraction. A previous study (Patek et al., 2004) proposed that elastic energy is stored as the saddle compresses into a more concave shape.

(Link 4, Fig. 2) remains contracted throughout the release phase (Burrows, 1969); contracted muscles are commonly used in biological linkage systems as fixed-length links (e.g. Muller, 1987; Westneat, 1990; Westneat, 1994). Pivot A is a fixed pivot point located at the meral-V articulation and located between Links 1 and 2. Pivot B is not fixed in space and is formed by the lateral meral-carpal articulation between Links 2 and 3. Pivot C also is not fixed in space and is located at the lateral extensor apodeme attachment on the carpus between Links 3 and 4. Pivot D is a fixed pivot formed by the lateral extensor muscle attachment immediately proximal to the saddle between Links 4 and 1 (there are no muscle attachments to the saddle itself).

Relative link lengths, as measured from photographs of resting appendages and video images of loaded appendages, were statistically indistinguishable with the exception of Link 4 (Table 1). As described above, Link 4 is formed by the contracted extensor muscle and thus is relaxed in the photographs and contracted in the video images of loaded appendages. Link 4 was an average of 14% shorter in an appendage prepared to strike as compared to a resting appendage. The mean starting angle between Links 1 and 2 was 64±5° (± s.d.; mean median 64°; range 40–77°; 24 video sequences, 6 individuals, 1–6 videos per individual).

Based on the average link lengths and starting angles measured in the high-speed video sequences, we developed an average four-bar model to generate predictions with which to compare the high-speed video data (Figs 9, 10, 11). This four-bar model is operational when input angles range from 63–99° and the input angles used by the mantis shrimp most often range from 64–73°. Within this limited range of input angles, the model output can be approximated as a line with a slope of 3.56 (least-squares linear regression, R^2=0.9970, P<0.0001) (Fig. 10). In other words, the model predicts a greater than threefold amplification of an input rotation (Fig. 11). This slope is equivalent to the predicted KT (kinematic transmission) of the system and was used to test whether the measured KT was correlated with predicted KT.

We compared the slope of the stomatopod kinematic input/output angles to the predicted slope of the four-bar model (3.56) (Figs 10, 11). The slope of the net rotation of input and output angles was 1.9 (intercept, 7.9; s.e.m., 0.2; 95%

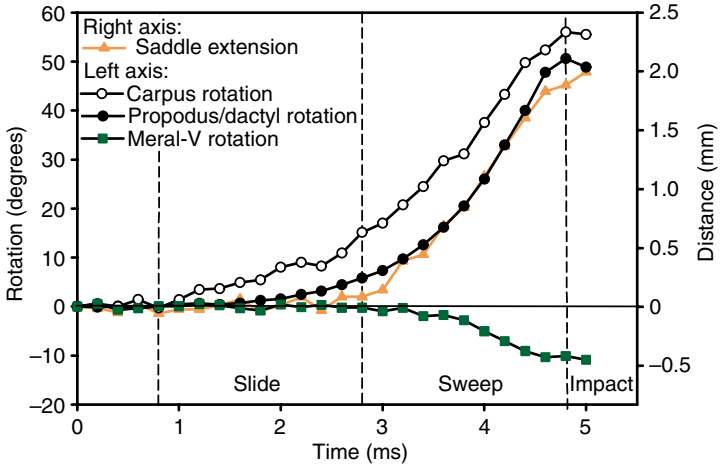

Fig. 7. The release phase of a smashing raptorial strike, illustrating the flexion and rotation of the raptorial appendage structures. The left axis represents rotation in degrees of the meral-V (green squares), propodus/dactyl unit (filled circles) and carpus (open circles). The right axis shows the length change of the saddle (orange triangles). Time zero is the end of the load phase, during which time the lateral extensor muscle contracted to rotate and close the meral-V and compress the saddle. The initial stages of the raptorial strike begin with a sliding movement in which the carpus rotates but the other segments move only slightly. The sweep phase begins when the meral-V rotates and saddle lengthens concurrently with the greatest angular acceleration of the carpus and propodus/dactyl. When impact occurs, the dactyl/propodus recoil while the saddle and meral-V continue to extend slightly. Data points were digitized from high-speed video images.

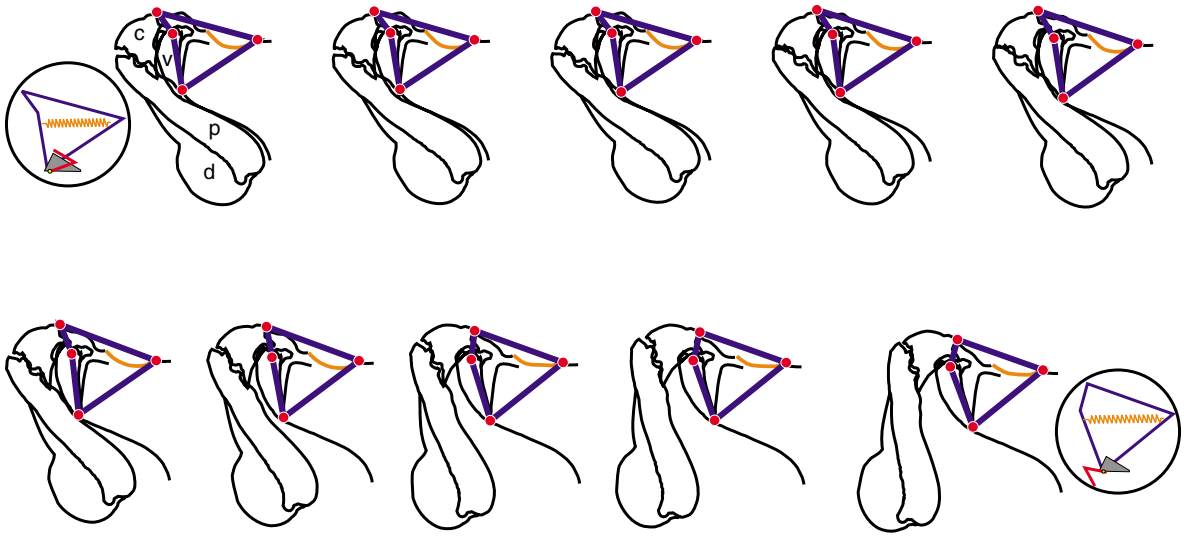

Fig. 8. A tracing of a typical strike sequence from high-speed video images with the links and pivots of a four-bar linkage mechanism overlaid on the tracings. Shown from left to right, images are 0.4 ms apart with the exception of the final two images, which are 0.2 ms apart. The saddle is colored orange; v, meral-v; c, carpus; p, propodus; d, dactyl. Insets illustrate schematically the compression and release of a spring (orange) and the braced and released position of sclerite 2 (red sclerite, gray brace).

confidence interval, 1.5–2.4; general linear model incorporating individual effects, R^2=0.8233; rotation, F=73.14, P<0.0001; individual effects, F=0.8588, P=0.51), which was significantly different from the predicted 3.56 slope of the model (t=–7.245; P<0.0001). Similarly, if the regression of the digitized data was constrained to a zero y-intercept, the slope of the net rotation input and output angles was significantly different than predicted by the four-bar model (slope, 2.6; s.e.m., 0.11; 95% confidence interval, 2.4–2.9; individual effects, F=1.50, P=0.24; t-test against four-bar model slope, t=–8.04, P<0.0001).

A four-bar linkage might work over the full 360° rotation of the input link, but that requires a certain set of linkage lengths. A more likely outcome is that that the model is ‘operational’ over a small range of input angles and ‘jams’ at either end of this range. We found that inter-individual variation in link lengths did not change the shape of the model curve substantially; however, the operational range of input angle values shifted substantially (Fig. 9). The input range over which the four-bar is operational if the relaxed extensor lengths are used as Link 4 was from 64° to 82° (mean ± s.d., 74±5°). When that link is contracted, however, as it is before the strike, the operational range was from 40° to 75° (mean 63±9°). The input angles for the contracted Link 4 measured from the video images were not significantly different than those predicted by the model (one-way ANOVA; F=0.5214, P=0.5), whereas when the relaxed Link 4 was used, the input angles were significantly different from the model predictions (one-way ANOVA; F=17.22, P=0.0002) and from the digitized input angles (one-way ANOVA; F=22.04, P<0.0001). When the extensor muscle was relaxed, most of the low end of the operational range exceeded the meral-V input angles measured in the high-speed video sequences and predicted by the model. This means that, for most of the observed input angles, the linkage mechanism would not function when the extensor muscle is relaxed.

Discussion

The mantis shrimp’s raptorial appendage has been rightly described as ‘*one of the most highly specialized pieces of operational machinery evolved by a crustacean*’ [p. 392 (Burrows and Hoyle, 1972)]. Through the basic physical principles of power amplification, the raptorial appendage generates remarkable forces and speeds (Burrows, 1969; Patek and Caldwell, 2005; Patek et al., 2004). Our results show that

Table 1. *Relative link lengths in relaxed appendages (photographed specimens) versus loaded appendages (high-speed video images)*

	Link length (%)			Statistical difference between resting and loaded appendage link lengths	
	Overall mean	Relaxed	Loaded	t	P
Link 2	79	80	76	1.313	0.21
Link 3	21	20	24	–1.86	0.082
Link 4	122	130	116	3.43	0.0035*

Lengths are expressed as a percentage of the length of Link 1.
*Statistically significant difference (P<0.005).

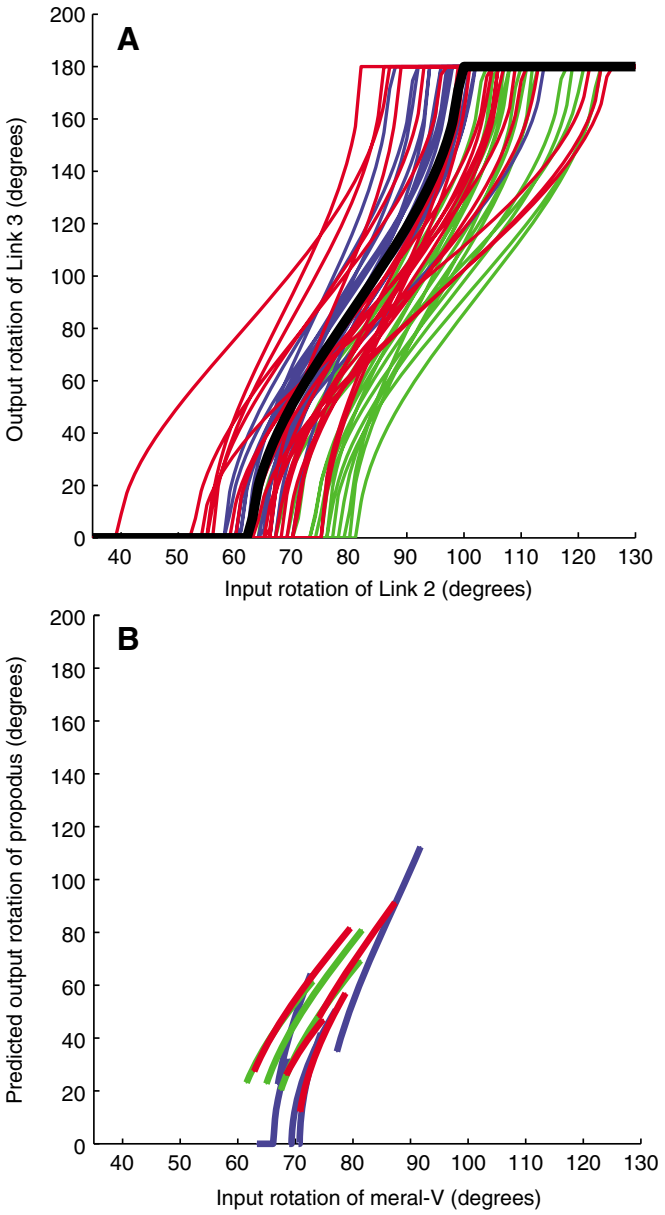

Fig. 9. The four-bar model predictions vary depending on relative link lengths and starting angles. The linkage mechanism is operational in two regions between input rotations of 0 and 360° (region from 0 to 180° shown; the range from 180–360° is the mirror image of 0 to 180° and is never used by mantis shrimp). The horizontal lines at output rotations of 0° and 180° indicate that a change in input rotation does not yield any output rotation (i.e. the linkage mechanism is non-operational). (A) An input rotation between 40° and 120° yields an output rotation depending on relative link lengths. Green traces show the predicted behavior based on the link lengths of a relaxed raptorial appendage (i.e. Link 4 extensor muscle is not contracted). Blue traces show the predicted behavior of the relaxed appendages if Link 4 is constrained to the average shortened length observed in video images. Red traces illustrate the range of behaviors given the range of link lengths measured in loaded appendages from video images. The thick black line provides the linkage model behavior given the average link lengths measured from the loaded images (red lines; also shown in Fig. 10). (B) The predicted model behavior of four individuals (each color represents a different individual) given measured inputs and link lengths from high-speed video sequences.

key modifications of the raptorial appendage's merus segment permit localized flexion, elastic energy storage and transmission of stored potential energy *via* linkages. Specifically, the meral-V both acts as an elastic energy storage device and one of the links in the linkage mechanism. In addition, the asymmetries in mineralization and joint architecture allow flexion of the lateral side of the merus that is offset by the constrained joint system and stiff exoskeleton of the medial side. A linkage mechanism is formed by the flexible components of the medial side, while a pair of sclerites controls the release of the strike by sliding against a simple brace formed by the merus exoskeleton. Thus, through the actuation of the strike by a pair of sclerites and the stabilization provided by the medial articulations and reinforcement of the merus, these animals can strike with remarkable precision to spear elusive fish or hammer hard-shelled molluscs (Caldwell and Dingle, 1976; Patek and Caldwell, 2005).

Stabilization and control: mineralization, articulations and sclerites

Analysis of the mineralization patterns in the merus and functional morphology of the joints provide new insights into the stabilization and articulations of the appendage. Arthropod appendages are usually perceived as a uniform series of hinged cylinders, yet CT scans (Figs 1, 3, 4) and kinematic analyses (Figs 7–9) revealed complex joints, distinct asymmetries in mineralization, and flexion on the lateral and medial sides of the merus (Fig. 6). For example, the lateral meral-carpal articulation couples the rotation of the meral-V to the carpus; in contrast, the medial meral-carpal articulations form a stabilizing channel, which restricts the carpus to dorsal/ventral movements (Fig. 5). Perhaps most surprising is the presence of a flexion point within the merus segment at the base of the rotatable meral-V; no equivalent flexion point exists on the opposite side of the merus. Instead, a thickened bar of exoskeleton on the medial side of the merus opposes the lateral flexion of the meral-V (Fig. 1). Thus, the dynamic linkages

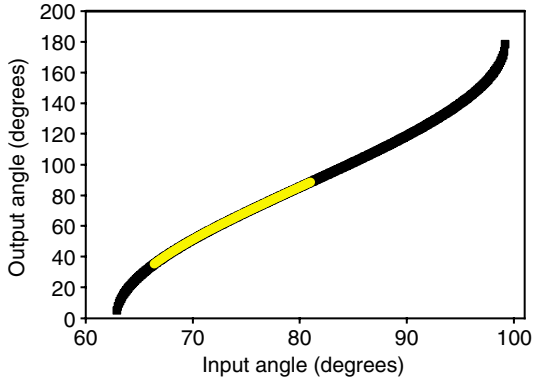

Fig. 10. Predicted four-bar model behavior based on the average link lengths of loaded raptorial appendages. For a given input angle, the four-bar linkage mechanism yields an output that varies nonlinearly along the range of input angles. The four-bar model is not operational beyond the range of input angles shown here. Kinematic analyses showed that mantis shrimp typically generate input angles of the meral-V in the range 64–73°, as indicated here (yellow line).

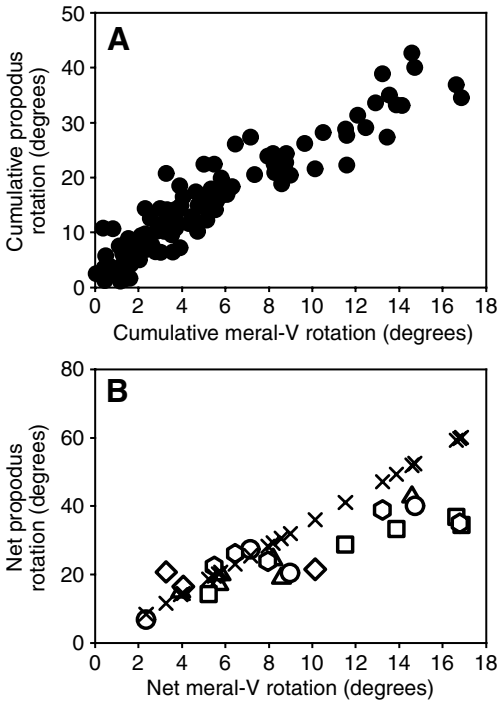

Fig. 11. The relationships between input angle rotation (Link 2, meral-V) and output angle rotation (Link 3, propodus rotation) measured in high-speed video sequences. (A) The cumulative change in input and output rotation across video frames (combined data from 23 strikes, five individuals). (B) The net input and output rotation (the total rotation across the full input range) across each strike recorded in the same individuals as in A, with each individual represented by a different symbol. The predicted output based on the four-bar model slope (crosses) is shown.

present on the lateral side are mirrored by a stiff medial wall of the merus, which lacks any flexion points.

The CT scans also permitted visualization of the highly mineralized sclerites. These images (Figs 3, 4) depicted the sclerites' orientation in an undisturbed specimen and suggested a somewhat different orientation and mechanism of action than previously proposed (Burrows, 1969). Rather than using a catch to lock the raptorial appendage during the loading phase, sclerite 2 slides smoothly over a bracing surface formed by an infolding of the merus (Figs 3, 4). Sclerite 1 folds above sclerite 2 and does not have a comparable bracing surface. The use of a smooth brace, rather than binary latch, explains why previous electromyographic analyses showed that both the extensor and flexor muscles remain contracted when the appendage is in a loaded state and why mantis shrimp typically hold the cocked position for only a brief time period (Burrows, 1969). This arrangement also permits mantis shrimp to disengage the system without firing; the extensor and flexor muscles can simply slowly relax to release the stored energy over a longer time period. At present, it is not clear whether the two sclerites have distinct functions or whether sclerite 1 simply serves to increase the mechanical advantage of the larger sclerite 2 (Burrows, 1969) relative to the considerable force generated by the opposing extensor muscle contraction.

These latches may be similar in origin to other latch systems in arthropods (reviewed in Gronenberg, 1996a). For example, trap-jaw ants generate extreme speeds and accelerations during their mandible strikes and have evolved latch systems multiple times using various modifications of joints and mouthparts (Gronenberg, 1995a; Gronenberg, 1995b; Gronenberg, 1996b; Gronenberg et al., 1998; Patek et al., 2006). The flea also uses modifications of the exoskeleton to lock a compressed block of resilin in place prior to a jump (Rothschild et al., 1975; Rothschild and Schlein, 1975). Similarly, the mantis shrimp's sclerites appear to be mineralized modifications of the flexor apodemes.

Transmission: kinematics and linkage mechanics

The raptorial strikes follow a characteristic series of movements, beginning with a brief, 0.9 ms 'slide phase' when the propodus slides several millimeters distally along the merus and no movement of external meral structures is visible (Figs 7, 8). Then, the saddle begins to lengthen, the meral-V rotates distally and the propodus, dactyl and carpus transition to a sweeping rotational movement (Figs 7, 8), which lasts an average 1.8 ms and brings the dactyl heel to an average speed of 14 m s^{-1} (609 rad s^{-1}). The magnitude and timing of the meral-V and propodus rotations are correlated, such that greater rotations of the propodus are correlated with larger meral-V rotations. Furthermore, the propodus rotates at least twice the meral-V rotation over the course of an entire strike (Fig. 11).

A four-bar linkage mechanism and the mechanical coupling proposed previously (Patek et al., 2004) are generally supported by the transmission of a twofold rotational amplification of the meral-V to the propodus (Figs 9–11). However, the KT of the empirical data is lower than predicted by the model, raising the question as to whether an alternative model should be considered or, instead, that the four-bar model is appropriate for the system and some additional effect is absorbing rotational input of the merus. For example, the incomplete fit of the model may be caused by non-planar orientation of linkages and the presence of a sliding cam-type joint between the merus and carpus (Fig. 5A); this joint could yield shifting force vectors or lever arms during meral-V rotation. Shifting mechanical advantage of the contracted extensor muscle relative to the relaxing flexor muscles during latch release (Burrows, 1969) may influence the momentum of the dactyl/propodus/carpus unit as it rotates around this point [e.g. in bush crickets (Burrows and Morris, 2003)]. In addition, Burrows noted that strike speeds were influenced by duration, frequency and timing of both flexor and extensor muscle activity (Burrows, 1969). Thus, this variable control of muscle activity could cause a change in length of Link 4, resulting in variable meral-V rotation and saddle-shortening, again influencing the output of the system (Fig. 9). All of these potential variations on the model should be addressed in future studies, and, although infrequently performed, alternative models to this four-bar linkage mechanism should be evaluated (e.g. Hoese and Westneat, 1996; Muller, 1996).

In most systems, a high KT is associated with high speeds, whereas a low KT is found in systems with large forces. Perhaps counter-intuitively, even with a relatively high KT of approximately 2, the high-speed system of *O. scyllarus* can also generate large forces. Such extreme accelerations, coupled with

an impact between two hard, massive surfaces, cause the strikes to yield high transient forces that can exceed 1000 N (Patek and Caldwell, 2005). Linkage systems that yield a high angular output rotation relative to input rotation are considered 'speed-modified'; however, mantis shrimp produce both high speeds and forces through extreme acceleration. Thus, these high transient forces are due to rotational amplification rather than a low KT.

One strength of evaluating linkage mechanics in an arthropod system is the ability to use exoskeletal markers during actual strikes, unlike vertebrate linkage systems in which the link lengths and positions have traditionally been limited to inferences from dissection and external soft markers. Specifically, we were able to measure the effects of varying Link 4 (formed by the contracted extensor muscle) as well as the range of input angles actually used by the mantis shrimp (Fig. 9). Link 4 was 14% shorter in contracted, loaded appendages than in relaxed appendages. When entered into the four-bar model, these longer link lengths yielded greater predicted input angles that were significantly different than the observed and predicted input angle range of a contracted Link 4 length (Fig. 9). Furthermore, we were able to measure actual input angles (Fig. 9) in order to evaluate the mechanical space within the model that is actually used by the mantis shrimp. Both of these approaches offered insights into the variability of the link lengths and input angles across and within individuals, suggesting that rotational amplification is robust across a range of parameters while, at the same time, yielding slightly different performance output.

The twofold KT found in mantis shrimp is high relative to four-bar linkages evaluated across fish which range, for example, from 0.5 to 1.29 in labrid fish jaws (Alfaro et al., 2004; Hulsey and Wainwright, 2002). In addition, some bony fishes may use a spring-loaded four-bar configuration by storing elastic energy in the linkage system and then relying on small shifts in relative position of the links to release the system (Muller, 1987). Surprisingly, we were unable to find any published arthropod systems in which a four-bar linkage mechanism has been analyzed.

Elastic energy storage

In a system as small as this one, the definitive determination of where elastic energy is being stored is challenging. Two factors determine storage capacity – the amount of deformation of an element and its stiffness. As in the crossbow, either character alone is not sufficient. Energy is not stored to an appreciable extent in the string; although it is bent at an acute angle, string has little flexural stiffness. There is also little energy stored in the stiff catch mechanism; it does not deform substantially. The energy storage is principally in the limbs of the bow; this can be shown by determining the mechanical properties of these structural elements and measuring their deflection when the bow is cocked. For the mantis shrimp strike, some deformations are too small to fully characterize from the video and the extent of mineralization offers a proxy for stiffness. Here we will propose a principal storage mechanism, but the testing of the mechanism awaits nanoindention studies and finer scale resolution of strain in the various parts of the merus.

Previous research suggested that elastic energy storage in the mantis shrimp system was provided by the extensor apodeme (Burrows, 1969), saddle (Patek et al., 2004) and unspecified cuticular elements (Currey et al., 1982) (Fig. 6). Apodeme elasticity was calculated to be insufficient to power the extreme kinematics of these strikes (Patek et al., 2004) and it was suggested that the saddle could provide the additional needed power. We propose an additional or alternative energy storage structure: the meral-V. The poor mineralization of the saddle (Fig. 1) means that although the saddle is flexible, it is unlikely that a substantial amount of energy can be stored through conformational changes of this structure. Instead, elastic potential energy is probably stored *via* multiple sites of cuticular deformation, most likely concentrated in the meral-V (Fig. 6). Ultimately, to resolve this debate, mechanical and material tests must be made directly on the system as a whole and on each of these structures.

The shape of arthropod cuticle, as well as its composition, influences the presence and degree of elastic energy storage (Vincent, 1990; Vincent and Wegst, 2004; Wainwright et al., 1976). While the presence of resilin, the arthropod rubber-like protein (Weis-Fogh, 1960), has not yet been determined in this system, the shape of the meral-V suggests an elastic function. The meral-V and the ventral bar extending from its lateral flexion point resembles the human-engineered tape spring, i.e. a thin strip with a bend or fold at which elastic energy is stored (Seffen and Pellegrino, 1999; Vehar et al., 2004; Vincent and Wegst, 2004). The flexion point at the base of the meral-V is similar to the elastic bend in a tape spring and the poorly mineralized area adjacent to this bar should permit flexion (Fig. 1). Furthermore, when manipulated, the meral-V strongly resists flexion and springs back into an open position when released. The saddle's function, given the intriguing hyperbolic–paraboloid shape and considerable flexion during the load phase, remains to be determined. Hyperbolic–paraboloid shells often are used in engineered systems to reduce local buckling through the presence of two opposite and transverse curves. Thus, the saddle may provide a flexible, yet strong, region of cuticle that allows the necessary space on the medial side of the merus equivalent to the amount of shortening occurring when the meral-V closes on the lateral side of the merus. However, while the meral-V is highly variable across stomatopods, the saddle is highly conserved, and retains its elegant, hyperbolic–paraboloid form across all mantis shrimp (R.L.C. and S.N.P., personal observation), thus suggesting an important, and as yet not fully determined, function.

The integration of elastic energy storage and force transmission through specialized joint articulations is a hallmark of arthropod power amplification systems (Bennet-Clark, 1975; Bennet-Clark, 1976a; Bennet-Clark, 1976b; Bennet-Clark and Lucey, 1967; Blickhan and Barth, 1985; Sensenig and Shultz, 2003). Not only is there a rich diversity of power amplification systems across arthropods, including fleas, locusts and snapping shrimp, but even within the mantis shrimp there is substantial morphological diversity of the saddle, meral-V and linkage articulations (S.N.P., personal observation) (Ahyong, 2001). Integrative analyses of the kinematics, material properties and conformational changes of these systems will continue to reveal

new insights into the origins and evolutionary diversification of powerful animal movements.

We thank Wyatt Korff, T. J. Kelleher, Sanjay Sane, Bill Kier, Dan Dudek, Matt McHenry, Charles Nunn, Mimi Koehl, the Hebets lab and the UC Berkeley Biomechanics Seminar for insightful comments and assistance. We also greatly appreciate the constructive comments from two anonymous reviewers. Special thanks to Tim Green, Tom Fitz and the British Broadcasting Corporation (BBC) Natural History Unit for their assistance with filming. Funding was provided by the BBC and the Miller Institute for Basic Research in Science (to S.N.P.).

References

Ahyong, S. T. (2001). *Revision of the Australian Stomatopod Crustacea*. Sydney: Australian Museum.

Alexander, R. M. (1983). *Animal Mechanics*. Boston: Blackwell Scientific Publications.

Alexander, R. M. (1990). Elastic mechanisms in the locomotion of vertebrates. *Neth. J. Zool.* **40**, 93-105.

Alexander, R. M. and Bennet-Clark, H. C. (1977). Storage of elastic strain energy in muscle and other tissues. *Nature* **265**, 114-117.

Alfaro, M. E., Bolnick, D. I. and Wainwright, P. C. (2004). Evolutionary dynamics of complex biomechanical systems: an example using the four-bar mechanism. *Evolution* **58**, 495-503.

Barel, C. D. N., van der Meulen, J. W. and Berkhoudt, H. (1977). Kinematischer transmissionskoeffizient und vierstangensystem als funktionsparameter und formmodel fur maandibulare depressionsapparate beiteleostiern. *Anat. Anz.* **142**, 21-31.

Bennet-Clark, H. C. (1975). The energetics of the jump of the locust *Schistocerca gregaria*. *J. Exp. Biol.* **63**, 53-83.

Bennet-Clark, H. C. (1976a). *Energy Storage in Jumping Animals*. Oxford, New York, Toronto, Sydney, Paris, Braunschweig: Pergamon Press.

Bennet-Clark, H. C. (1976b). Energy storage in jumping insects. In *The Insect Integument* (ed. H. R. Hepburn), pp. 421-443. Amsterdam: Elsevier.

Bennet-Clark, H. C. and Lucey, E. C. A. (1967). The jump of the flea: a study of the energetics and a model of the mechanism. *J. Exp. Biol.* **47**, 59-76.

Blickhan, R. and Barth, F. G. (1985). Strains in the exoskeleton of spiders. *J. Comp. Physiol. A* **157**, 115-147.

Burrows, M. (1969). The mechanics and neural control of the prey capture strike in the mantid shrimps *Squilla* and *Hemisquilla*. *Z. Vergl. Physiol.* **62**, 361-381.

Burrows, M. and Hoyle, G. (1972). Neuromuscular physiology of the strike mechanism of the mantis shrimp, *Hemisquilla*. *J. Exp. Zool.* **179**, 379-394.

Burrows, M. and Morris, O. (2003). Jumping and kicking in bush crickets. *J. Exp. Biol.* **206**, 1035-1049.

Caldwell, R. L. and Dingle, H. (1976). Stomatopods. *Sci. Am.* **1976**, 81-89.

Collar, D. C., Near, T. J. and Wainwright, P. C. (2005). Comparative analysis of morphological diversity: does disparity accumulate at the same rate in two lineages of centrarchid fishes. *Evolution* **59**, 1783-1794.

Currey, J. D., Nash, A. and Bonfield, W. (1982). Calcified cuticle in the stomatopod smashing limb. *J. Mater. Sci.* **17**, 1939-1944.

de Groot, J. H. and van Leeuwen, J. L. (2004). Evidence for an elastic projection mechanism in the chameleon tongue. *Proc. R. Soc. Lond. B Biol. Sci.* **271**, 761-770.

Deban, S. M., Wake, D. B. and Roth, G. (1997). Salamander with a ballistic tongue. *Nature* **389**, 27-28.

Grafen, A. and Hails, R. (2002). *Modern Statistics for the Life Sciences*. New York: Oxford University Press.

Gronenberg, W. (1995a). The fast mandible strike in the trap-jaw ant *Odontomachus* I. Temporal properties and morphological characteristics. *J. Comp. Physiol. A* **176**, 391-398.

Gronenberg, W. (1995b). The fast mandible strike in the trap-jaw ant *Odontomachus.* II. Motor control. *J. Comp. Physiol. A* **176**, 399-408.

Gronenberg, W. (1996a). Fast actions in small animals: springs and click mechanisms. *J. Comp. Physiol. A* **178**, 727-734.

Gronenberg, W. (1996b). The trap-jaw mechanism in the dacetine ants *Daceton armigerum* and *Strumigenys* sp. *J. Exp. Biol.* **199**, 2021-2033.

Gronenberg, W., Brandão, C. R. F., Dietz, B. H. and Just, S. (1998). Trap-jaws revisited: the mandible mechanism of the ant *Acanthognathus*. *Physiol. Entomol.* **23**, 227-240.

Heitler, W. J. (1974). The locust jump: specialisations of the metathoracic femoral-tibial joint. *J. Comp. Physiol.* **89**, 93-104.

Hoese, W. J. and Westneat, M. W. (1996). Biomechanics of cranial kinesis in birds: testing linkage models in the white-throated sparrow (*Zonotrichia albicollis*). *J. Morphol.* **227**, 305-320.

Hulsey, C. D. and Wainwright, P. C. (2002). Projecting mechanics into morphospace: disparity in the feeding system of labrid fishes. *Proc. R. Soc. Lond. B Biol. Sci.* **269**, 317-326.

Kunze, J. C. (1981). The functional morphology of stomatopod Crustacea. *Philos. Trans. R. Soc. Lond. B Biol. Sci.* **292**, 255-328.

Lappin, A. K., Monroy, J. A., Pilarski, J. Q., Zepnewski, E. D., Pierotti, D. J. and Nishikawa, K. C. (2006). Storage and recovery of elastic potential energy powers ballistic prey capture in toads. *J. Exp. Biol.* **209**, 2535-2553.

McNeill, P., Burrows, M. and Hoyle, G. (1972). Fine structures of muscles controlling the strike of the mantis shrimp, *Hemisquilla*. *J. Exp. Zool.* **179**, 395-416.

Muller, M. (1987). Optimization principles applied to the mechanism of neurocranium levation and mouth bottom depression in bony fishes (Halecostomi). *J. Theor. Biol.* **126**, 343-368.

Muller, M. (1996). A novel classification of planar four-bar linkages and its application to the mechanical analysis of animal systems. *Philos. Trans. R. Soc. Lond. B Biol. Sci.* **351**, 689-720.

Nishikawa, K. C. (1999). Neuromuscular control of prey capture in frogs. *Philos. Trans. R. Soc. Lond. B Biol. Sci.* **354**, 941-954.

Patek, S. N. and Caldwell, R. L. (2005). Extreme impact and cavitation forces of a biological hammer: strike forces of the peacock mantis shrimp (*Odontodactylus scyllarus*). *J. Exp. Biol.* **208**, 3655-3664.

Patek, S. N., Korff, W. L. and Caldwell, R. L. (2004). Deadly strike mechanism of a mantis shrimp. *Nature* **428**, 819-820.

Patek, S. N., Baio, J. E., Fisher, B. F. and Suarez, A. V. (2006). Multifunctionality and mechanical origins: ballistic jaw propulsion in trap-jaw ants. *Proc. Natl. Acad. Sci. USA* **103**, 12787-12792.

Ritzmann, R. (1973). Snapping behavior of the shrimp *Alpheus californiensis*. *Science* **181**, 459-460.

Rothschild, M. and Schlein, Y. (1975). The jumping mechanism of *Xenopsylla cheopis*. I. Exoskeletal structures and musculature. *Philos. Trans. R. Soc. Lond. B Biol. Sci.* **271**, 457-490.

Rothschild, M., Schlein, J., Parker, K., Neville, C. and Sternberg, S. (1975). The jumping mechanism of *Xenopsylla cheopis* III. Execution of the jump and activity. *Philos. Trans. R. Soc. Lond. B Biol. Sci.* **271**, 499-515.

Seffen, K. A. and Pellegrino, S. (1999). Deployment dynamics of tape springs. *Proc. R. Soc. Lond. A Math. Phys. Sci.* **455**, 1003-1048.

Sensenig, A. T. and Shultz, J. W. (2003). Mechanics of cuticular elastic energy storage in leg joints lacking extensor muscles in arachnids. *J. Exp. Biol.* **206**, 771-784.

Uicker, J. J., Jr, Pennock, G. R. and Shigley, J. E. (2003). *Theory of Machines and Mechanisms*. New York: Oxford University Press.

Vehar, C., Kota, S. and Dennis, R. (2004). Closed-loop tape springs as fully compliant mechanisms – preliminary investigations. In *Proceedings of the DETC 2004, International Design Engineering Technical Conference*. Salt Lake City, Utah.

Versluis, M., Schmitz, B., von der Heydt, A. and Lohse, D. (2000). How snapping shrimp snap: through cavitating bubbles. *Science* **289**, 2114-2117.

Vincent, J. (1990). *Structural Biomaterials*. Princeton: Princeton University Press.

Vincent, J. F. V. and Wegst, U. G. K. (2004). Design and mechanical properties of insect cuticle. *Arthropod Struct. Dev.* **33**, 187-199.

Wainwright, S. A., Biggs, W. D., Currey, J. D. and Gosline, J. M. (1976). *Mechanical Design in Organisms*. Princeton: Princeton University Press.

Walker, J. A. (1998). Estimating velocities and accelerations of animal locomotion: a simulation experiment comparing numerical differentiation algorithms. *J. Exp. Biol.* **201**, 981-995.

Weis-Fogh, T. (1960). A rubber-like protein in insect cuticle. *J. Exp. Biol.* **37**, 889-907.

Westneat, M. W. (1990). Feeding mechanics of teleost fishes (Labridae; Perciformes): a test of four-bar linkage models. *J. Morphol.* **205**, 269-295.

Westneat, M. W. (1991). Linkage biomechanics and evolution of the unique feeding mechanism of *Epibulus insidiator* (Labridae: Teleostei). *J. Exp. Biol.* **159**, 165-184.

Westneat, M. W. (1994). Transmission of force and velocity in the feeding mechanisms of labrid fishes (Teleostei, Perciformes). *Zoomorphology* **114**, 103-118.

Westneat, M. W. (1995). Feeding, function, and phylogeny: analysis of historical biomechanics in labrid fishes using comparative methods. *Syst. Biol.* **44**, 361-383.

Westneat, M. W., Long, J. H., Jr, Hoese, W. and Nowicki, S. (1993). Kinematics of birdsong: functional correlation of cranial movements and acoustic features in sparrows. *J. Exp. Biol.* **182**, 147-171.